Optimal fast-response sliding-mode control for flexible-substrate measurement

Bor-Jiunn Wen [a,b], T.S. Liu [a,*]

[a] Department of Mechanical Engineering, National Chiao Tung University, Hsinchu 30010, Taiwan
[b] Center for Measurement Standards, Industrial Technology Research Institute, Hsinchu 30011, Taiwan

ARTICLE INFO

ABSTRACT

In order to control bending radii of flexible substrates in displays, this paper presents an optimal fast-response sliding-mode control method. Maximum driving voltages are utilized in sliding-mode control based on a linear quadratic estimator. An optimal design for the threshold value and the reaching-law parameter are obtained by using a procedure of the fast-response regulation. Implementing the proposed method, this study measures electrical resistances for different widths of line patterns on polyethylene terephthalate/indium tin oxide substrates up to 11,000 bending times.

© 2013 Elsevier Ltd. All rights reserved.

1. Introduction

With rapid advance in semiconductor technology as well as in electronic display industry, the digital household appliances are becoming more and more diversified. However, hard electronic products can not satisfy people who demand comfortable and convenient lifestyle. The flexible electronics, which is thin and flexible, shock-resistant, and not limited by the occasion or space, will become the top choice of consumer electronic products. The inspection technique of flexible electronic products is not mature. Therefore, Grego, Lewis, Vick, and Temple (2005) provided two methods for bending-test technique. But there are some limiting factors when using the methods. The purpose of this study is to put forward a new control technique for measuring bending characteristics of flexible electronics under different bending radii by using a flexible-characteristics inspection system (FCIS). FCIS was designed to exert an external force on the flexible electronics. It resulted in a curved screen and made the flexible electronics crooked. Hence, this study shot the crooked states of flexible displays using a charge-coupled device (CCD), and carried out image processing using a LabVIEW software, calculated the bending radius of the flexible electronics (Gonzalez & Woods, 2008; Wen, Liu, Chen, Ko, & Chung, 2008). In mass and rapid inspections, there are various sizes and thin film layers in different flexible electronics products. Since parameters of FCIS mathematical model are different every time due to variable

boundary conditions of each flexible electronics, the mathematical model is highly nonlinear. Therefore, in order to achieve stable bending-radius control, a controller is designed in the present study.

In constructing ARX models, according to Verhaegen and Verdult (2007), a cyclic manner of iteratively refining data from real-life measurements identifies model parameters for an unknown dynamical system. To carry out bending-radius control on FCIS in this study, a mathematical model of a FCIS mechanism is first identified by an ARX model (Peng, Ozaki, Toyoda, & Oda, 2001). Secondly, a control-algorithm design is developed according to results of FCIS plant identification. Simulation results obtained by CCD feedback signals are used to calculate the bending radius. Thirdly, the architecture of the control algorithm is integrated on FCIS to implement bending-radius control for measuring electrical characteristics of flexible electronics. Nevertheless, the mathematical model of FCIS is highly nonlinear, and there are also uncertainties and disturbance in FCIS. There are a lot of well-known control methods, e.g. fuzzy control, neural control, sliding-mode control (SMC) and so on. Compared to SMC, it takes a lot of time to obtain the parameters in neural control by multilayer neural network learning (Lin & Lee, 1999). Fuzzy control requires more system responses to design a good membership function. According to the experimental results (Chung, Wen, & Lin, 2007), the performance of SMC is better than fuzzy control in the presence of systemic uncertainties and disturbances. Because SMC is effective in dealing with systemic uncertainties and disturbances (Alfaro-Cid, McGookin, Murray-Smith, & Fossen, 2005; Edwards & Tan, 2006), an advanced SMC algorithm is developed in this study. In addition, iterative learning control (ILC) may improve the transient response and tracking

---

* Correspondence to: 1001 Ta-Hsueh Road, Hsinchu 30010, Taiwan.
Tel.: +886 35712121x55123; fax: +886 35720634.
E-mail address: tsliu@mail.nctu.edu.tw (T.S. Liu).

performance of uncertain dynamic systems that operate repetitively (Xu, Panda, & Lee, 2009). According to a brief and categorization of ILC (Ahn, Chen, & Moore, 2007), there are two kinds of technical papers about ILC. One is related to the literature that focuses on ILC applications (Chen & Moore, 2002; Dou, Tan, Lee, & Zhou, 1999; Wu & Liu, 2004), and the other is related to the literature focused on the theoretical developments (Chien, 2000; Chen, Moore, & Bahl, 2004; Jiang & Unbehauen, 2002). Briefly, ILC is an intelligent control methodology (Abdallah, Soualian, & Schamiloglu, 1998) for improving the transient performance of systems that operate repetitively over a fixed time interval. Messner, Horowitz, Kao, and Boals (1991) compensated the nonlinear properties of plant and disturbance by using learning estimation. However, iterative learning estimations require more time to compute control inputs. As a result, to achieve a robust and fast-response control system for various kinds of flexible electronics, an optimal fast-response sliding-mode control (OFRSMC) is presented in this study with simulations and experiments for measuring electrical characteristics of flexible electronics. The new technique measures electrical characteristics of flexible polyethylene terephthalate (PET)/indium tin oxide (ITO) substrates up to 11,000 bending times from flat to 2 cm bending radius by using FCIS based on the OFRSMC. In addition, this study measures resistances for 5, 10, 20, 30, 40, and 50 dpi widths of the line pattern on PET/ITO samples. If resistances of flexible electronics increase a lot after bending tests, flexible electronics probably will not work. According to inspection results, a designer or maker of flexible electronics can design useful and comfortable flexible electronic products for human being.

2. Measurement apparatus of flexible-characteristics inspection system

In order to measure electrical characteristics of the flexible electronics, this study puts forward the flexible-characteristics inspection system, as depicted in Fig. 1, which comprises a clip unit, a flexible-characteristics inspection stage with a motor, a motion controller, a computer, and a CCD camera. In addition, the clip unit is configured with two clipping arms which can work cooperatively for holding a flexible electronic substrate. In order to bend the flexible substrate in pure bending, this study designed an opposite moving of the two clipping arms in the round moving simultaneously to implement. The sever motor drives the flat belt pulley and the spur gear pair in the same speed simultaneously. The flat belt pulley and the spur gear pair link up different clipping arms, respectively. The transmission speed from the server motor to flat belt pulley is the same as to spur gear pair, but in opposite directions respectively. Therefore, both clipping arms can make an opposite movement of the two clipping arms in the circular path at the same moving speed simultaneously. Moreover, because there is only a bending force on the perpendicular direction of the flexible substrate by clipping arms, an opposite movement of the two clipping arms in the circular path simultaneously can make a pure bending for testing the flexible substrate.

Moreover, to measure the electrical-resistance characteristics, a 4-point-probe electrical-resistance measurement apparatus is integrated into two clipping arms, as shown in Fig. 2. Measurement errors concerning the electrode-contact electrical-resistance can hence be reduced by using the principle of the 4-point-probe electrical-resistance measurement (Meier & Levinzon, 1965). In this study, the flexible substrate is sheet-like or plate-like object.

3. Design and simulation of optimal fast-response sliding-mode control

3.1. Design of optimal fast-response sliding-mode control

FCIS depicted in Fig. 1 is a nonlinear system. Real-world nonlinear control problems are dealt with by different techniques (Cheng & Li, 1998; Li & Shieh, 2000). The model of FCIS can be
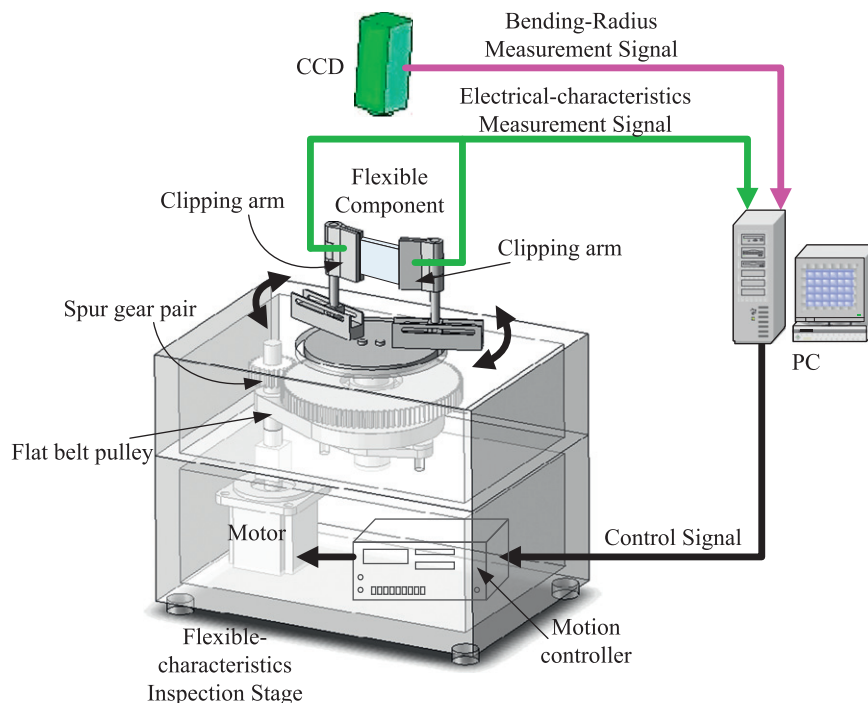

Fig. 1. Schematic diagram of flexible-characteristics inspection system.
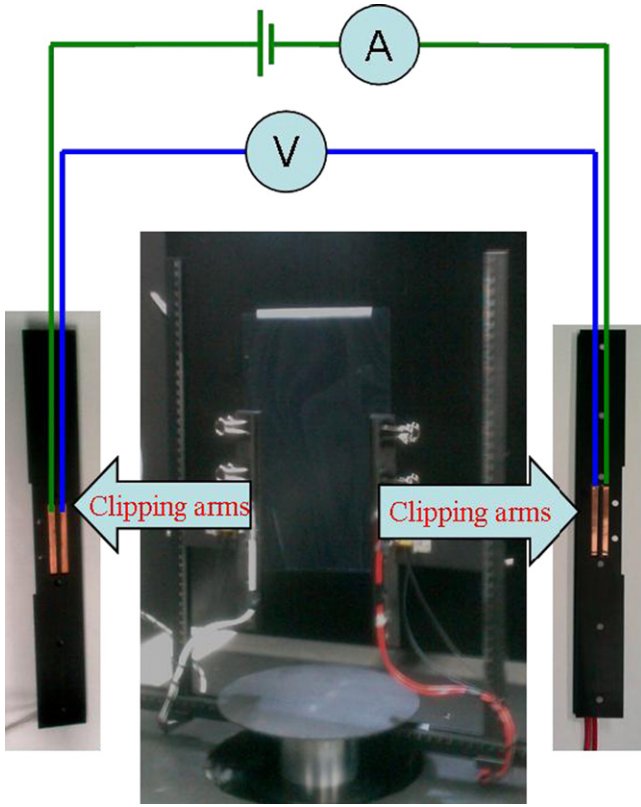
Fig. 2. Four-point-probe electrical-resistance measurement apparatus.

identified by an ARX model as

$$y(k) = \frac{b_1 h^{-1} + \cdots + b_n h^{-n}}{1 + a_1 h^{-1} + \cdots + a_n h^{-n}} u(k) + \frac{1}{1 + a_1 h^{-1} + \cdots + a_n h^{-n}} e(k) \tag{1}$$

where h is the shift operator, $e(k) \in R$ is a zero-mean white-noise sequence that is independent from $u(k) \in R$, and a_i and b_i are real-valued scalars (Verhaegen & Verdult, 2007). According to Fig. 1, FCIS includes a motor, a flat belt pulley, a spur gear pair, clipping arms, and a flexible substrate. Therefore, a frequency-sweep input sequence (Verhaegen & Verdult, 2007) is utilized to set up an identification experiment in this study. Accordingly, the transfer function that relates the control voltage $V(z)$ to the bending curvature $Y(z)$ can be obtained in state-variables form

$$\begin{cases} X(k+1) = A_z X(k) + B_z u(k) \\ y(k) = C_z X(k) \end{cases} \tag{2}$$

where $X(k) \in R^n$ is the state variables of system, $u(k) \in R^m$ is the input voltage of the motion controller and $y(k) \in R^r$ is the assumed model output related to the bending radius of the flexible substrate on FCIS.

Sliding-mode control's robust and disturbance-insensitive characteristics enable the SMC to perform well in systems with model uncertainty, disturbances and noises. In this paper, SMC is utilized to design the control input voltage of the motion controller. To design SMC, a sliding function is designed first, and then enforces a system trajectory to enter sliding surface in a finite time. As soon as the system trajectory enters the sliding surface, it moves along the sliding surface to a control goal. To sum up, there are two procedures of sliding mode. The proposed SMC is based on pole placement (Chang, 1999), since the sliding function can be designed by pole placement. Some conditions

are prescribed set for the sliding vector design in the proposed sliding-mode control:

1. $\text{Re}\{\lambda_i\} < 0$, $\alpha_j \in R$, $\alpha_j < 0$, $\alpha_j \neq \lambda_i$.
2. Any eigenvalue in $\{\alpha_1, \ldots, \alpha_m\}$ is not in the spectrum of A_z.
3. The number of any repeated eigenvalues in $\{\lambda_1, \ldots, \lambda_{n-m}, \alpha_1, \ldots, \alpha_m\}$ is not greater than m, the rank of B_z, where $\{\lambda_1, \lambda_2, \ldots, \lambda_{n-m}\}$ are sliding-mode eigenvalues and $\{\alpha_1, \alpha_2, \ldots, \alpha_m\}$ are virtual eigenvalues.

As proved by Sinswat and Fallside (1977), if the condition (3) in the above is established, the control system matrix $A_z - B_z K$ can be diagonalized as

$$A_z - B_z K = \begin{bmatrix} V \\ F \end{bmatrix}^{-1} \begin{bmatrix} \Phi_V & 0 \\ 0 & \Gamma_F \end{bmatrix} \begin{bmatrix} V \\ F \end{bmatrix} \tag{3}$$

where $\Phi_V = \text{diag}[\lambda_1, \lambda_2, \ldots, \lambda_{n-m}]$, $\Gamma_F = \text{diag}[\alpha_1, \alpha_2, \ldots, \alpha_m]$, and V and F are left eigenvectors with respect to Φ_V and Γ_F, respectively. Hence, Eq. (3) can be rewritten as

$$\begin{cases} V(A_z - B_z K) = \Phi_V V \\ F(A_z - B_z K) = \Gamma_F F \end{cases} \tag{4}$$

rearrangement of Eq. (4) yields

$$FA_z - \Gamma_F F = (FB_z)K \tag{5}$$

according to Chang (1999),

$$\text{rank}(FA_z - \Gamma_F F) = \text{rank}(F) \tag{6}$$

since F contains m independent left eigenvectors, one has $\text{rank}(F) = m$. From Eqs. (5) and (6), it is also true that $\text{rank}(FA_z - \Gamma_F F) = \text{rank}((FB_z)K) = \text{rank}(F) = m$. In other words, FB_z is invertible. With the designed left eigenvector F above, the sliding function $S(k)$ is designed as

$$S(k) = FX(k) \tag{7}$$

The second step is the discrete-time switching control design. A different and much more expedient approach than that of Gao and Hung (1993) is adopted here. This control law is called the reaching law approach that has been proposed for continuous variable structure control (VSC) systems (Hung, Gao, & Hung, 1993). This control law is synthesized from the reaching law in conjunction with a plant model and the known bounds of perturbations. For a discrete-time system, the reaching law is (Gao, Wang, & Homaifa, 1995)

$$S(k+1) - S(k) = -qTS(k) - \varepsilon T\text{sgn}(S(k)) \tag{8}$$

where $T > 0$ is the sampling period, $q > 0$ is the reaching-law parameter, $\varepsilon > 0$ is the sliding-layer thickness and $1 - qT > 0$. Therefore, the switching control law for the discrete-time system is derived based on this reaching law. From Eq. (7), $S(k)$ and $S(k+1)$ can be obtained in terms of sliding vector F as,

$$\begin{cases} S(k) = FX(k) \\ S(k+1) = FX(k+1) = FA_z X(k) + FB_z u(k) \end{cases} \tag{9}$$

it follows that:

$$S(k+1) - S(k) = FA_z X(k) + FB_z u(k) - FX(k) \tag{10}$$

from Eqs. (8) and (10),

$$\begin{aligned} S(k+1) - S(k) &= -qTS(k) - \varepsilon T\text{sgn}(S(k)) \\ &= FA_z X(k) + FB_z u(k) - FX(k) \end{aligned}$$

solving for $u_{sc}(k)$ gives the switching control law

$$u_{sc}(k) = -(FB_z)^{-1}[FA_z X(k) + (qT - 1)FX(k) + \varepsilon T\text{sgn}(FX(k))] \tag{11}$$

In order to achieve the output tracking control, a reference command input $r(k)$ is introduced into the system by modifying a state feedback control law $u_p(k) = -KX(k)$ with pole-placement design method (Franklin, Powell, & Workman, 1998) to become

$$u_p(k) = N_u r(k) - K(X(k) - N_x r(k)) \tag{12}$$

where $K \in R^n$ is a gain matrix obtained by assigning n desired eigenvalues $\{\lambda_1, \ldots, \lambda_{n-m}, \alpha_1, \ldots, \alpha_m\}$ of $A_z - B_z K$ and

$$\begin{bmatrix} N_u \\ N_x \end{bmatrix} = \begin{bmatrix} A_z - I & B_z \\ C_z & 0 \end{bmatrix}^{-1} \begin{bmatrix} 0 \\ I \end{bmatrix} \tag{13}$$

The proposed SMC input, based on Eq. (12), is assumed to be

$$u_S(k) = u_p(k) + u_{sc}(k) = N_u r(k) - K(X(k) - N_x r(k)) + u_{sc}(k) \tag{14}$$

substituting Eq. (11) into (14) gives the proposed SMC input as

$$u_S(k) = N_u r(k) - K(X(k) - N_x r(k)) - (FB_z)^{-1}[FA_z X(k) \\ + (qT-1)FX(k) + \varepsilon T \operatorname{sgn}(FX(k))] \tag{15}$$

The pole-placement SMC design method utilizes the feedback of all the state variables to form the desired sliding vector. In practice, not all the state variables are available for direct measurement. It is necessary to estimate the state variables that are not directly measurable. Therefore, the SMC input depicted in Eq. (15) is rewritten as

$$u_S(k) = N_u r(k) - K(\tilde{X}(k) - N_x r(k)) - (FB_z)^{-1}[FA_z \tilde{X}(k) \\ + (qT-1)F\tilde{X}(k) + \varepsilon T \operatorname{sgn}(F\tilde{X}(k))] \tag{16}$$

where $\tilde{X}(k)$ is an observed state. Define a full-order estimator (FOE) as

$$\begin{cases} \tilde{X}(k+1) = A_z \tilde{X}(k) + B_z u(k) + K_e(y(k) - C_z \tilde{X}(k)) \\ \tilde{y}(k) = C_z \tilde{X}(k) \end{cases} \tag{17}$$

and K_e is an observer feedback gain matrix.

Image noise in CCD feedback signals is an error factor in controlling a bending radius. Hence, a linear quadratic estimator (LQE) is applied here to estimate optimal states. Based on Eq. (2), consider a system model

$$\begin{cases} X(k+1) = A_z X(k) + B_z u(k) + Gv(k) \\ y(k) = C_z X(k) + \omega(k) \end{cases} \tag{18}$$

where $X(k) \in R^n$ is the state variable, $u(k) \in R^m$ is the control input voltage, $y'(k) \in R^r$ is the assumed plant output related to the bending radius, and $v(k) \in R^n$ and $\omega(k) \in R^r$ are system disturbances and measurement noise with covariances $E[\omega \omega^T] = Q$, $E[vv^T] = R$, and $E[\omega v^T] = 0$. The objective of LQE is to find a vector $\hat{X}(k)$, which is an optimal estimation of the present state $X(k)$. Here "optimal" means the cost function (Franklin et al., 1998; Phillips & Nagle, 1995)

$$J = \lim_{T \to \infty} E \left\{ \int_0^T (X^T Q X + u^T R u) dt \right\} \tag{19}$$

is minimized. The solution is an estimator written as

$$\begin{cases} \hat{X}(k+1) = A_z \hat{X}(k) + B_z u(k) + K_f(y(k) - C_z \hat{X}(k)) \\ \hat{y}(k) = C_z \hat{X}(k) \end{cases} \tag{20}$$

where K_f is the "optimal Kalman" gain $K_f = PC_z^T R^{-1}$ and P is the solution of the algebraic Riccati equation

$$A_z P + PA_z^T - PC_z^T R^{-1} C_z P + Q = 0 \tag{21}$$

SMC and LQE are integrated into a so called optimal sliding-mode control (OSMC) with control input

$$u_{OS}(k) = N_u r(k) - K(\hat{X}(k) - N_x r(k)) - (FB_z)^{-1}[FA_z \hat{X}(k) \\ + (qT-1)F\hat{X}(k) + \varepsilon T \operatorname{sgn}(F\hat{X}(k))] \tag{22}$$

In order to expedite the response time, the maximum driving voltage control is utilized in OSMC by a fast-response regulator, whose input is written as

$$u_F(k) = \tfrac{1}{2} U_{\max}[\operatorname{sgn}(|r(k)| - \Phi) + 1] - \tfrac{1}{2}[\operatorname{sgn}(|r(k)| - \Phi) - 1] \\ [N_u r(k) - K(X(k) - N_x r(k)) - (FB_z)^{-1}[FA_z X(k) \\ + (qT-1)FX(k) + \varepsilon T \operatorname{sgn}(FX(k))]] \tag{23}$$

where Φ is a threshold value of the reference command input. When $|r(k)|$ is larger than Φ, $\operatorname{sgn}(|r(k)| - \Phi) = 1$. Therefore, the proposed input is

$$u_F(k) = \tfrac{1}{2} U_{\max}[1+1] - \tfrac{1}{2}[1-1][N_u r(k) - K(X(k) - N_x r(k)) \\ - (FB_z)^{-1}[FA_z X(k) + (qT-1)FX(k) + \varepsilon T \operatorname{sgn}(FX(k))]] = U_{\max} \tag{24}$$

as a consequence, the maximum driving voltage $U_{\max}$ is applied. However, when $|r(k)|$ is less than Φ, $\operatorname{sgn}(|r(k)| - \Phi) = -1$. Therefore, the proposed input becomes

$$u_F(k) = \tfrac{1}{2} U_{\max}[-1+1] - \tfrac{1}{2}[-1-1][N_u r(k) - K(X(k) - N_x r(k)) \\ - (FB_z)^{-1}[FA_z X(k) + (qT-1)FX(k) + \varepsilon T \operatorname{sgn}(FX(k))]] \\ = N_u r(k) - K(X(k) - N_x r(k)) - (FB_z)^{-1}[FA_z X(k) \\ + (qT-1)FX(k) + \varepsilon T \operatorname{sgn}(FX(k))] \tag{25}$$

In Eq. (23), both threshold value Φ and reaching-law parameter q affect response speed. In addition, boundary conditions of each flexible electronics are different and the mathematical model is a nonlinear model for controlling the bending radius. In order to achieve a fast-response and robust bending-radius control, an optimal design for Φ and q is vital. Therefore, fast response regulation is developed in this study to obtain Φ and q optimally, so that the maximum driving voltage is applied in the early control period. Assume a nonlinear output written as

$$y(k) = ae^{bk} \tag{26}$$

taking the logarithm to both sides of Eq. (26) yields

$$\ln y(k) = \ln a + bk \tag{27}$$

the best-fit values (Perl, 1960) are thus

$$a = e^{\left(\sum_{k=1}^n k^2 \sum_{k=1}^n \ln y(k) - \sum_{k=1}^n k \sum_{k=1}^n k\ln y(k))/n \sum_{k=1}^n k^2 - \left(\sum_{k=1}^n k \right)^2 \right)} \tag{28}$$

$$b = \frac{n \sum_{k=1}^n k\ln y(k) - \sum_{k=1}^n k \sum_{k=1}^n \ln y(k)}{n \sum_{k=1}^n k^2 - (\sum_{k=1}^n k)^2} \tag{29}$$

in terms of a and b parameters, the predictive arrival time k_r is obtained as

$$k_r = \frac{\ln R_i - \ln a}{b} \tag{30}$$

where R_i is a command input. Then, the threshold value for the maximum driving voltage input is obtained as

$$\Phi = ae^{bs_r k_r} \tag{31}$$

where s_r is a ratio parameter for minimum sliding-mode time and the threshold value has to be no smaller than εT. Then, reaching-law parameter q is also obtained as

$$q = \frac{1 - \Phi}{T} \tag{32}$$

therefore, according to a procedure of the fast-response regulation from Eq. (28) to (32), the threshold value and reaching-law parameter can be obtained. The system block diagram is shown in Fig. 3 where R_i is a input signal of the bending radius. In the beginning, the maximum driving voltage is applied to control a bending radius. A CCD provides the bending-radius feedback signal for LQE, which can estimate optimal states in the presence of system disturbances and measurement noise in SMC. After
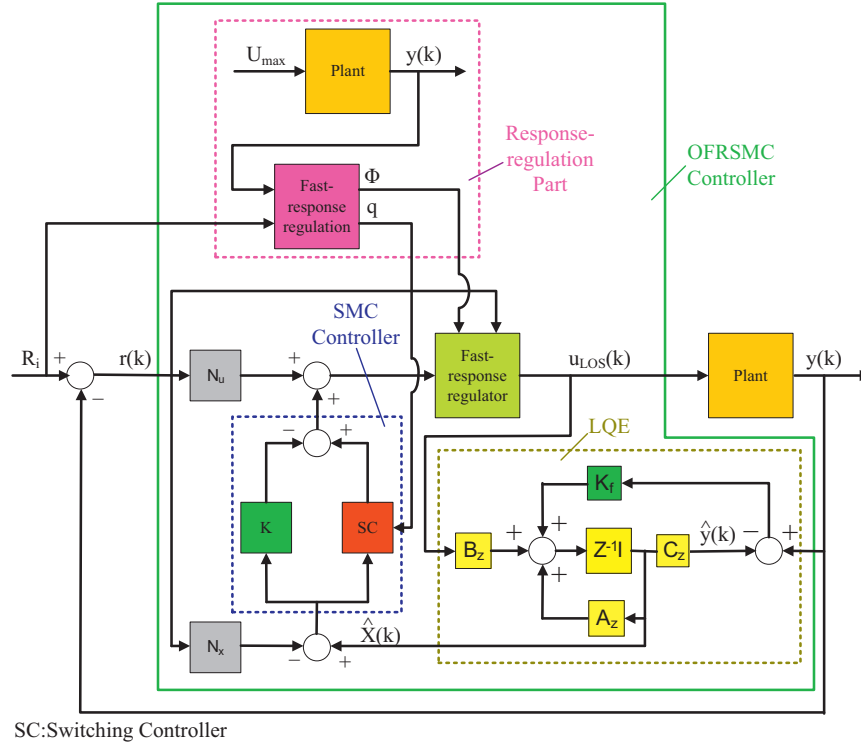
Fig. 3. System block diagram.

several control cycles, the threshold value and the reaching-law parameter are obtained by the fast-response regulation. Finally, the SMC with the fast-response regulator and LQE can implement the bending-radius control robustly. According to Eqs. (22) and (23), a new controller called optimal fast-response sliding-mode control (OFRSMC) is expressed by

$$u_{ORS}(k) = \tfrac{1}{2} U_{max} \big[\mathrm{sgn}(|r(k)| - \varPhi) + 1 \big] - \tfrac{1}{2} \big[\mathrm{sgn}(|r(k)| - \varPhi) - 1 \big]$$
$$[N_u r(k) - K(\hat{X}(k) - N_x r(k)) - (FB_z)^{-1}[FA_z \hat{X}(k)$$
$$+ (qT - 1)F\hat{X}(k) + \varepsilon T \mathrm{sgn}(F\hat{X}(k))]] \tag{33}$$

OFRSMC will be carried out in simulations and experiments, which are presented in Section 3.3 and Section 4.1, respectively.

3.2. Stability analysis of OFRSMC

This section deals with a system model described by Eq. (2) and defines a reference command input $r(k)$. To overcome the nonlinear control problem, the model of FCIS is identified by an ARX model. A motor provides driving frequencies varying up to 0.2 Hz for bending frequencies from negative to positive bending, and bending radii of substrates are measured in real time by CCD images, as shown in Fig. 1. The sampling time T is 0.08 s. All the parameters of the FCIS described by the ARX model are obtained by using a cyclic manner of iteratively refining data (Verhaegen & Verdult, 2007) from bending-radius measurements. Accordingly, the transfer function that relates the control voltage $V(z)$ and the bending radius $Y(z)$ can be written as

$$H(z) = \frac{Y(z)}{V(z)} = \frac{0.10361z^2 - 0.14046z + 0.06742}{z^3} \tag{34}$$

in addition, the transfer function of FCIS can be rewritten in state-variables form. Accordingly, $A_z = \begin{bmatrix} 0 & 0 & 0 \\ 1 & 0 & 0 \\ 0 & 1 & 0 \end{bmatrix}$, $B_z = \begin{bmatrix} 1 \\ 0 \\ 0 \end{bmatrix}$ and $C_z = \begin{bmatrix} 0.10361 & -0.14046 & 0.06742 \end{bmatrix}$ are obtained for Eq. (2).

In this study, Ackermann's formula (Ackermann, 1972) is used to determine the pole-placement feedback gain matrix $K = \begin{bmatrix} -0.08 & 0.0017 & 0.00001 \end{bmatrix}$. The pole-placement algorithm described in Section 3.1 is utilized to determine a sliding vector $F = \begin{bmatrix} 0.99756 & -0.06983 & 0.001 \end{bmatrix}$. In practice, the fact that not all state variables are available for direct measurement results in the necessity to estimate the state variables that are not measurable. Hence, the FOE designed by Ackermann's formula and LQE are utilized in this study, where the observer feedback gain matrix is

$$K_e = \begin{bmatrix} -0.05933 \\ 6.0022 \\ -6.8346 \end{bmatrix}$$ and the optimal Kalman gain is

$$K_f = \begin{bmatrix} 1.9193 \\ -1.7375 \\ 0.66094 \end{bmatrix},$$ respectively. In addition, according to Eq. (13),

N_u and N_x are obtained as $[32.712]$ and $\begin{bmatrix} 32.712 \\ 32.712 \\ 32.712 \end{bmatrix}$, respectively.

In order to analyze the stability of FCIS with the OFRSMC, Lyapunov analysis (Slotine & Li, 1991) and a proof method by contradiction (Andrilli & Hecker, 2009) is utilized. Consider a discrete-time quadratic Lyapunov function candidate

$$V_L(X(k)) = X^*(k)\Omega X(k) \tag{35}$$

where Ω is a given symmetric positive definite matrix. Differentiating the positive definite function $V_L(X(k))$ along the system trajectory yields another quadratic form

$$\Delta V_L(X(k)) = V_L(X(k+1)) - V_L(X(k)) = X^*(k)(A_s^*\Omega A_s - \Omega)X(k)$$
$$= -X^*(k)\Lambda X(k) \tag{36}$$

where

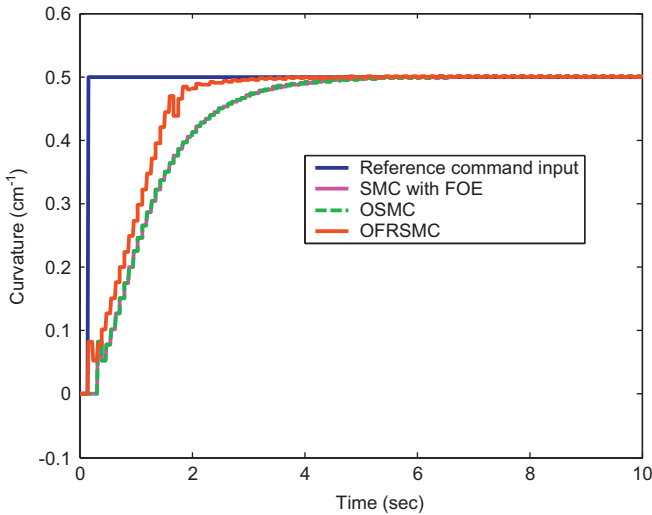$$A_s^*\Omega A_s - \Omega = -\Lambda \tag{37}$$

Fig. 4. Simulation results of FCIS in controlling the flexible substrate at 0.5 cm^{-1} bending curvature without random measurement noise. The blue solid line represents command input, the magenta solid line is the system output based on SMC with FOE, the green broken line is the system output based on OSMC, and the red solid line is the system output based on OFRSMC. (For interpretation of the references to color in this figure legend, the reader is referred to the web version of this article.)

is called a Lyapunov equation and A_s is a system state matrix with a control method. If both Ω and Λ are both positive definite matrices satisfying Eq. (37), the system is globally asymptotically stable. Therefore, according to the OFRSMC law, when $|r(k)|$ is larger than Φ, Eq. (33) is rewritten as

$$u_{LOS}(k) = U_{max} \qquad (38)$$

substituting Eq. (38) into (2) gives the model of FCIS with the OFRSMC as

$$\begin{cases} X(k+1) = A_z X(k) + B_z U_{max} \\ y(k) = C_z X(k) \end{cases} \qquad (39)$$

where $A_z = A_s$. According to a proof method by contradiction, firstly assume that Eq. (39) is unstable. Eq. (37) is rewritten as

$$A_z{}^* \Omega A_z - \Omega = -\Lambda \qquad (40)$$

let $\Lambda = I$ and denote Ω as a symmetric matrix. The solution Ω in Eq. (40) is $\begin{bmatrix} 1 & 6.6613e^{-16} & 1.6177e^{-16} \\ 6.6613e^{-16} & 2 & 2.433e^{-15} \\ 1.6177e^{-16} & 2.433e^{-15} & 3 \end{bmatrix}$. According to Sylvester's criterion (Ogata, 1994), Ω is positive definite. The solution Ω contradicts the assumption that the model of FCIS with the OFRSMC when $|r(k)| - \Phi > 0$ is unstable.

On the other hand, when $|r(k)|$ is less than Φ, Eq. (33) is rewritten as

$$u_{LOS}(k) = -K\hat{X}(k) - (FB_z)^{-1} FA_z \hat{X}(k) = -(K + (FB_z)^{-1} FA_z)\hat{X}(k) \qquad (41)$$

where $qT \cong 1$ and $\varepsilon T \to 0$. Substituting Eq. (41) into (2) gives the model of FCIS with the OFRSMC as

$$\begin{cases} \hat{X}(k+1) = A_z\hat{X}(k) - B_z(K + (FB_z)^{-1} FA_z)\hat{X}(k) = (A_z - B_z(K + (FB_z)^{-1} FA_z))\hat{X}(k) = A_s\hat{X}(k) \\ \hat{y}(k) = C_z\hat{X}(k) \end{cases} \qquad (42)$$

according to a proof method by contradiction, assume that Eq. (42) is unstable. Eq. (37) is rewritten as

$$(A_z - B_z(K + (FB_z)^{-1} FA_z))^* \Omega(A_z - B_z(K + (FB_z)^{-1} FA_z)) - \Omega = -\Lambda \qquad (43)$$

let $\Lambda = I$ and denote Ω as a symmetric matrix. The solution Ω in
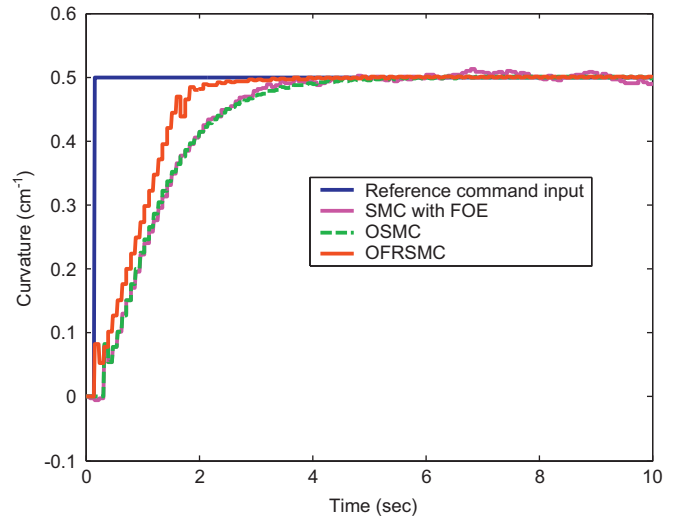

Fig. 5. Simulation results of FCIS in controlling the flexible substrate at 0.5 cm^{-1} bending curvature with random measurement noise. The blue solid line represents command input, the magenta solid line is the system output based on SMC with FOE, the green broken line is the system output based on OSMC, and the red solid line is the system output based on OFRSMC. (For interpretation of the references to color in this figure legend, the reader is referred to the web version of this article.)

Eq. (43) is $\begin{bmatrix} 1.02290 & 0.15302 & 0.01749 \\ 0.15302 & 2.02290 & 0.15302 \\ 0.01749 & 0.15302 & 3.02290 \end{bmatrix}$. According to Sylvester's criterion (Ogata, 1994), Ω is positive definite. The solution Ω contradicts the assumption that the model of FCIS with the OFRSMC when $|r(k)| - \Phi < 0$ is unstable. Therefore, FCIS with the OFRSMC is asymptotically stable in the large.

3.3. Simulation of OFRSMC

In simulations, random disturbances of 10% input signal in magnitude are exerted on the system plant. Because image noise in CCD feedback signals is an important error factor in bending radius control, random measurement noises of 10% input signal in magnitude are exerted on CCD feedback signals. Figs. 4 and 5 show simulation results of FCIS in controlling the flexible substrate at 0.5 cm^{-1} bending curvature based on SMC with the FOE, OSMC, and OFRSMC without and with random measurement noise by using MATLAB and Simulink, respectively. In Figs. 4 and 5, the blue solid line represents command input, the magenta solid line is the system output based on SMC with FOE, the green broken line is the system output based on OSMC, and the red solid line is the system output based on the OFRSMC. In addition to parameters of the control system in Section 3.2, the reaching-law parameter q is 12.4 and the sliding-layer thickness ε is 1.25 in the simulation based on SMC with FOE and OSMC. In the simulation based on OFRSMC, the maximum driving voltage is applied in the first five control cycles. According to the five control-cycle data and the fast-response regulation, $a = 0.045$, $b = 2.1$, $k_r = 1.147$, $s_r = 0.33$, the threshold value $\Phi = 0.1$ and the reaching-law parameter $q = 11.25$ are obtained.

In this study, to evaluate the system performance, integrated absolute error (IAE) that is often of practical significance is used as the performance index and is expressed as

$$IAE = \int_0^{T_F} |e(t)| dt \qquad (44)$$

where $e(t)$ is a error function of the plant and T_F is a finite time (Franklin et al., 1998). The integral of time multiplied by absolute error (ITAE) that provides the performance index of the best sensitivity is expressed as

$$\text{ITAE} = \int_0^{T_F} t|e(t)|dt \qquad (45)$$

where $e(t)$ is a error function of the plant and T_F is a finite time (Franklin et al., 1998). According to the simulated results shown in Figs. 4 and 5, the performance of three control systems in controlling the flexible substrate at 0.5 cm^{-1} bending curvature are evaluated by using IAE and ITAE indices and the results, are shown in Table 1.

In addition, Fig. 6 depicts simulation results of FCIS with random measurement noise in controlling the flexible substrate at 0.25 cm^{-1} bending curvature based on SMC with FOE, OSMC, and OFRSMC repeatedly. In Fig. 6(a), (b) and (c), the blue solid lines represent command inputs, the red solid lines are the system outputs by using SMC with FOE, OSMC, and OFRSMC, respectively.

Table 1
IAE and ITAE indices of simulation results for the control systems based on SMC with FOE, OSMC, and OFRSMC in controlling the flexible substrate at 0.5 cm^{-1} bending curvature without and with random measurement noise.

	Without random measurement noise		With random measurement noise	
	IAE	ITAE	IAE	ITAE
SMC with FOE	7.3082	8.1117	7.4636	9.5385
OSMC	7.3082	8.0873	7.3053	8.1127
OFRSMC	5.2747	4.6069	5.2912	4.7158

The following conclusions can be arrived at from the analysis of simulation results from Figs. 4 to 6 and Table 1:

1. According to Fig. 4, there are no overshoot without random measurement noise by using the three controllers. Because in controlling bending radius the overshoot situation is not allowed, We succeed in designing the three controllers. However, according to Figs. 5 and 6, there are overshoots in the control performances by using SMC with FOE controller. In Table 1, the control performances without and with random measurement noise based on SMC with FOE controller are obviously worse than the other two. Accordingly, the control performance of SMC with LQE is better than SMC with FOE in overcoming measurement noise.

2. In Fig. 6, one bending cycle using either SMC with FOE or OSMC needs 12 s, whereas using the OFRSMC needs 8 s only. Accordingly, there are more bending cycles in 36 s by using the OFRSMC method than by using SMC with FOE and OSMC.

3. Form simulation results, the response time for the bending-radius control based on the OFRSMC is the shortest among the three controllers. And the response time by using the OFRSMC is almost half time by using SMC with FOE or OSMC. In Table 1, the control performances based on the OFRSMC are obviously better than the other two. Therefore, the bending-radius on FCIS based on the OFRSMC performs better than that based on SMC with FOE, or the OSMC. It is certain that the OFRSMC method is capable of fast controlling the bending radius of flexible substrate on FCIS robustly and successfully. Section 4 depicts experimental results of controlling the bending radius of flexible substrates on FCIS based on SMC with FOE, OSMC, and OFRSMC, respectively.
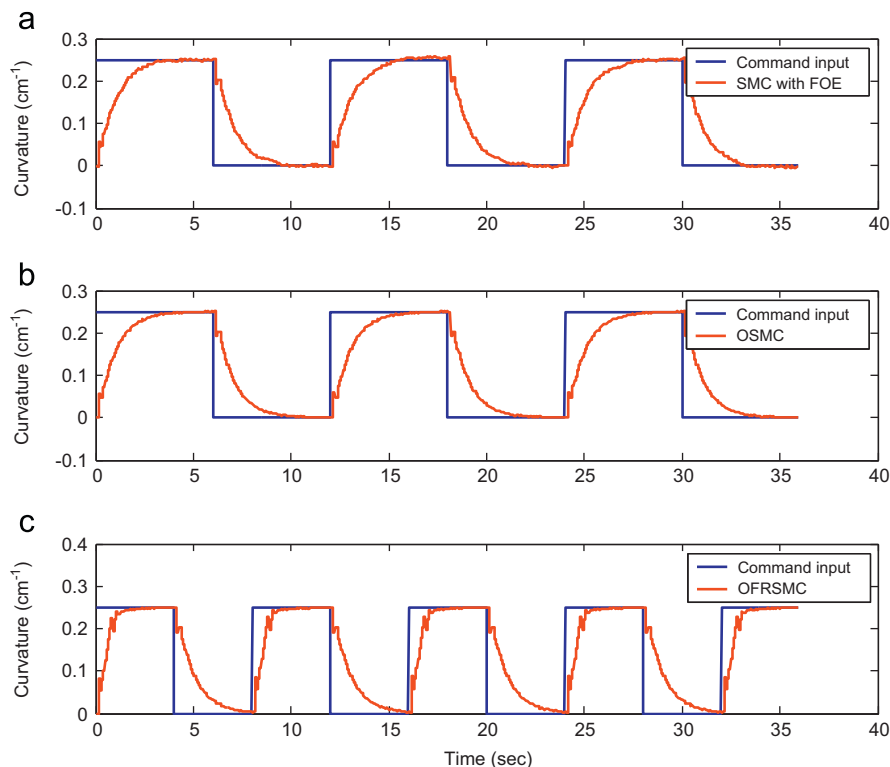

Fig. 6. Simulation results of FCIS with random measurement noise in controlling the flexible substrate at 0.25 cm^{-1} bending curvature repeatedly. Blue solid lines represent command input, and red solid lines are the system output based on (a) SMC with FOE, (b) OSMC and (c) OFRSMC. (For interpretation of the references to color in this figure legend, the reader is referred to the web version of this article.)

4. Experimental results

4.1. Experimental results of OFRSMC

In order to measure electrical characteristics of flexible electronics under different radii of curvature, a commercially available ITO-coated PET (OCTM 100) from CPFilms Inc. is utilized. A laser writer is utilized to make line patterns of different widths on a PET/ITO sample for a flexible back plate, which is used to drive the display media. SMC with FOE, OSMC, and OFRSMC control the bending radius at 2 cm respectively and the bending-radius control results are shown in Fig. 7. In addition, Fig. 8 compares experimental results of FCIS in controlling the flexible substrate at 4 cm bending radius based on SMC with the FOE, OSMC, and OFRSMC repeatedly. In experiments, parameters of SMC with FOE and OSMC in simulations are utilized. In the
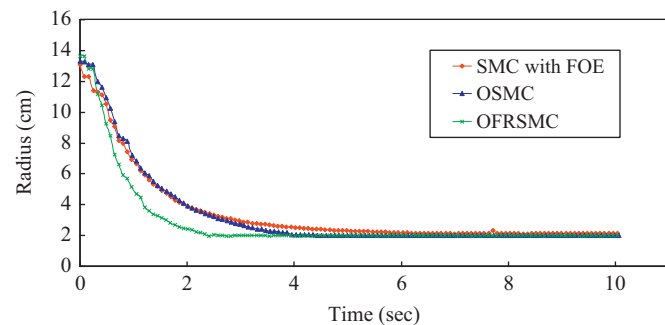
experiment based on OFRSMC, the maximum driving voltage is applied in the first five control cycles. By using five control-cycle data and the fast-response regulation, $a=0.072$, $b=0.566$, $k_r=3.424$, $s_r=0.3$, the threshold value $\Phi=0.129$ and the reaching-law parameter $q=10.89$ are obtained. According to the experimental results shown in Fig. 7, the performances of the three control systems in controlling the flexible substrate at 2 cm bending radius are evaluated by using IAE and ITAE indices and the results are shown in Table 2.

The following conclusions are drawn from experimental results:

1. According to Fig. 7 and Table 2, there appears no overshoot by using the three controllers. The performance of bending-radius control based on the OFRSMC is better than that based on SMC with FOE and OSMC, because the OFRSMC is more effective in overcoming system disturbances and measurement noise.
2. In Fig. 8, three-cycle bending operations by using SMC with FOE, OSMC, and the OFRSMC need 37 s, 36 s, and 17 s, respectively. Due to fast-response-regulation capability of the OFRSMC, the three-cycle bending period based on the OFRSMC is the shortest among the three controllers.
3. In a manner similar to simulation results, the OFRSMC response is the fastest and the most robust in view of Figs. 7 and 8 and Table 2. Compared to SMC with FOE and

Fig. 7. Experimental results of FCIS in controlling the flexible PET/ITO substrates at 2 cm bending radius. The red solid line is the system output based on SMC with FOE, the blue solid line is the system output based on OSMC, and the green solid line is the system output based on OFRSMC. (For interpretation of the references to color in this figure legend, the reader is referred to the web version of this article.)

Table 2
IAE and ITAE indices of experimental results for the control systems based on SMC with FOE, OSMC, and OFRSMC in controlling the flexible substrate at 2 cm bending radius.

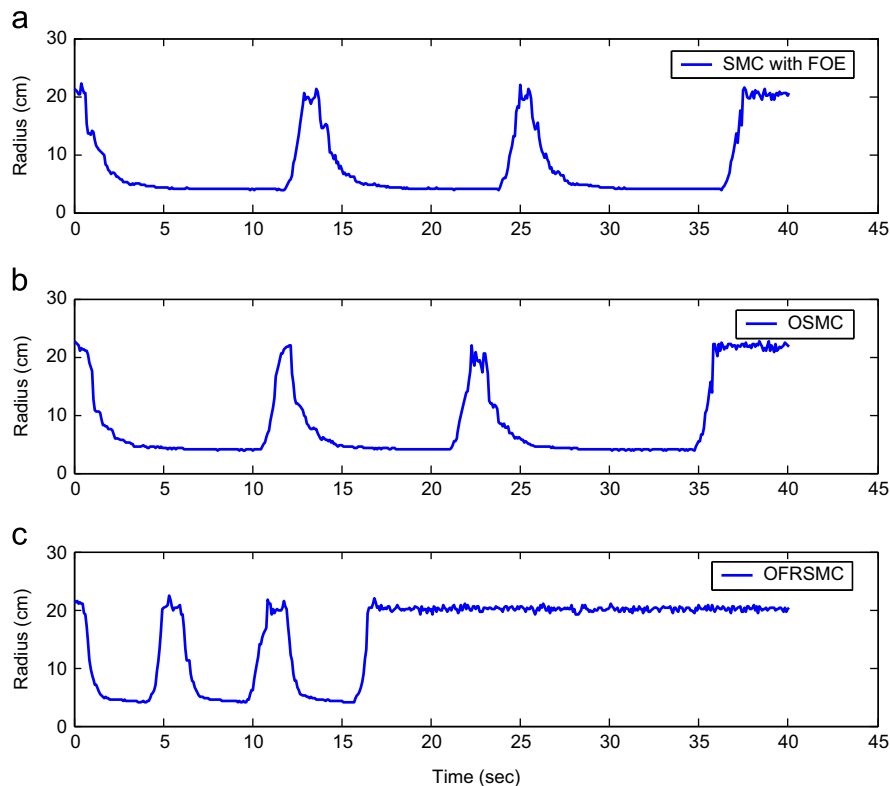|	IAE	ITAE
SMC with FOE	183.95	264.66
OSMC	173.00	154.35
OFRSMC	113.52	55.70

Fig. 8. Experimental results of FCIS in controlling the flexible substrate at 4 cm bending radius repeatedly based on (a) SMC with FOE, (b) OSMC and (c) OFRSMC.
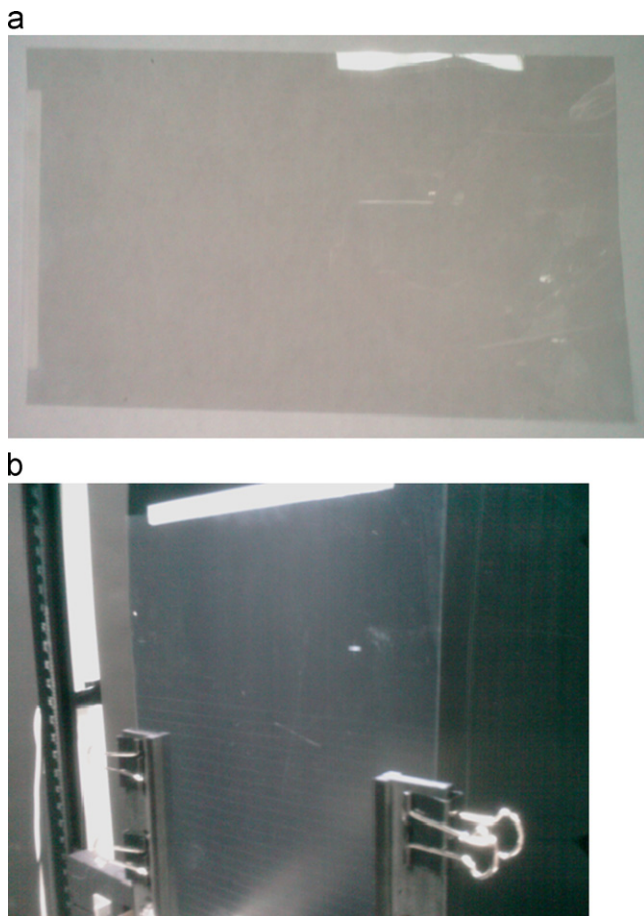
a

b

Fig. 9. (a) The entire picture, (b) zoom-in picture with electrodes of 5 dpi width of the line pattern on a PET/ITO sample.

OSMC, OFRSMC can overcome variable parameters, nonlinearity and measurement noise to achieve a better bending-radius control. Since experimental and simulation results are in good agreement, it is concluded that the OFRSMC outperforms the other two methods. Therefore, it is certain that the OFRSMC method is capable of bending-radius control on FCIS for fast and robustly measuring electrical characteristics in bending.

4.2. Measurement results of electrical characteristics of flexible substrate in bending

According to the experimental results given in Section 4.1, FCIS could be utilized for measuring bending characteristics of flexible electronics under different bending radii, as it successfully provides a more stable and robust bending condition by using the OFRSMC method for measuring electrical characteristics of flexible electronics.

Therefore, in order to measure electrical characteristics of flexible substrate under different radii of curvature, a commercially available ITO-coated PET (OCTM 100) from CPFilms Inc. is utilized. It has 50 nm think ITO on 125 μm think PET sheet. A laser writer is used in this work to make different widths of the line pattern on the PET/ITO sample. For example, Fig. 9 shows a 5 dpi width of the line pattern on a PET/ITO sample. The length and width of the line pattern are 152 mm and 5 mm, respectively. Therefore, by using FCIS based on the OFRSMC the method of 4-point-probe electrical-resistance measurement is applied for
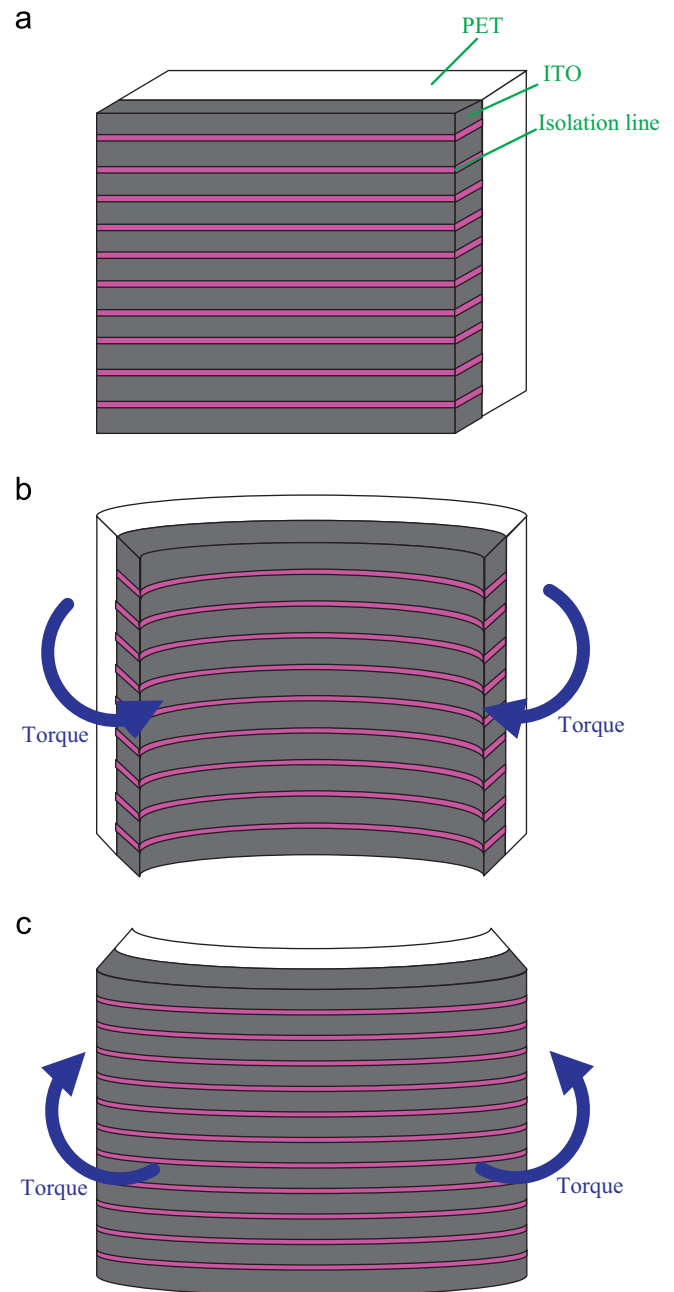
a

Fig. 10. Flexible PET/ITO sample is (a) flat, (b) compressive bending, and (c) tensile bending for ITO layer by force *F*; where white, gray and magenta color represent PET, ITO layer and isolation line, respectively. (For interpretation of the references to color in this figure legend, the reader is referred to the web version of this article.)

measuring the electrical resistance of the line pattern in flat and 2 cm bending radius conditions.

There are two types for bending a flexible substrate. One is the compressive bending, which means the bending direction makes ITO layers compressed, whereas the other is tensile bending. For example, Fig. 10(a), (b), and (c) depicts that ITO layers in flexible PET/ITO sample are in flat, compressive bending, and tensile bending, respectively. A one-time bending cycle by using FCIS based on the OFRSMC is to control from flat, 2 cm bending radius, and return to flat. Therefore, a 50 dpi PET/ITO sample was measured in flat and 2 cm compressive-bending radius conditions, respectively, for bending 11,000 times by using FCIS based on the OFRSMC, as shown in Table 3. In addition, this study

Table 3
Electrical-resistance measurement and change-rate of electrical resistance of 50 dpi flexible PET/ITO sample in flat and 2 cm bending radius conditions after 11,000 times compressive bending.

| Bending times	Bending conditions					
	Flat			2 cm Bending radius		
	Bending radius (cm)	Resistance (kΩ)	Change-rate of electrical resistance (%)	Bending radius (cm)	Resistance (kΩ)	Change-rate of electrical resistance (%)
0	∞	20.976	0.000	2.01	20.983	0.000
500	∞	21.046	0.334	2.00	21.058	0.357
1000	∞	21.063	0.415	2.05	21.071	0.419
2000	∞	21.082	0.505	2.02	21.093	0.524
3000	∞	21.100	0.591	2.05	21.108	0.596
4000	∞	21.110	0.639	2.05	21.116	0.634
5000	∞	21.117	0.672	2.04	21.125	0.677
6000	∞	21.126	0.715	2.01	21.131	0.705
7000	∞	21.129	0.729	2.04	21.136	0.729
8000	∞	21.131	0.739	2.05	21.139	0.743
9000	∞	21.135	0.758	2.05	21.145	0.772
10,000	∞	21.140	0.782	2.05	21.150	0.796
11,000	∞	21.145	0.806	2.03	21.149	0.791
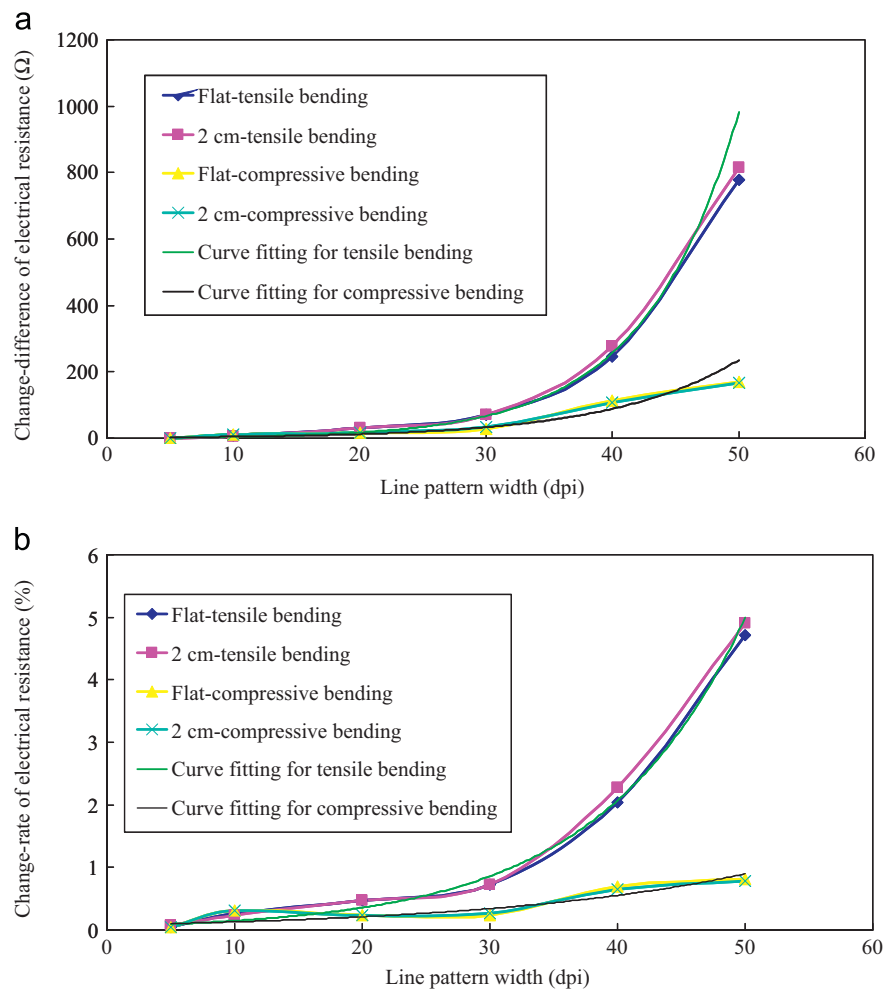
Fig. 11. (a) Change-difference of electrical resistance and (b) change-rate of electrical resistance after 11,000 times tensile and compressive bending for 5, 10, 20, 30, 40, and 50 dpi PET/ITO samples, respectively.

measures the electrical resistance for different widths of the line pattern on the sample up to 11,000 bending times. Fig. 11 depicts the change-difference and change-rate of electrical resistance after 11,000 times tensile and compressive bending for 5, 10, 20, 30, 40, and 50 dpi samples, respectively, where change-differences are calculated from the difference of the electrical resistance of the line pattern between before and after bending, and change-rates are calculated from the difference of the electrical resistance of the line pattern between before and after bending divided by the electrical resistance of the line pattern

before bending. According to measurement results, the following conclusions are drawn:

1. Table 1 depicts that the sample resistance with 2 cm bending radius is larger than the flat one, because the ITO-line pattern becomes thinner in bending. In addition, it also depicts that as the bending times increase, change-rates of electrical resistance in both flat and 2 cm bending radius conditions also increase.
2. In Table 1, both results of the flat and 2 cm bending radius conditions are similar.
3. Decreasing the width of the line pattern also increases change-rates of the resistance in both flat and 2 cm bending radius conditions.
4. As a consequence, tensile and compressive bending curve-fitting equations are respectively written as

$$C_d = 1.1148e^{0.137w} \tag{46}$$

$$C_d = 1.8368e^{0.097w} \tag{47}$$

where C_d is the change-difference of resistance between before and after 11,000 bending times, and w is the width of line patterns on the PET/ITO samples. According to Fig. 11 and both Eqs. (46) and (47), the relationship between the width of the line pattern and the change-rate of electrical resistance is exponential. In addition, this study obtains change-rate curve fitting equations for tensile and compressive bendings

$$C_r = 0.0613e^{0.088w} \tag{48}$$

$$C_r = 0.0806e^{0.0482w} \tag{49}$$

where C_r is the change-rate of electrical resistance between before and after 11,000 bending times, and w is the width of line patterns on the PET/ITO samples. From Fig. 11 and both Eqs. (48) and (49), the relationship between the width of the line patterns and the change-rate of electrical resistance is also exponential.
5. According to measurement results for two bending types, the increasing rate for the change-difference or the change-difference of resistance in tensile bending is higher than in compressive bending when decreasing the line pattern width.

5. Conclusions

This study has presented a stable, robust, and fast-response bending-radius condition of flexible substrates by using FCIS based on the OFRSMC. This study also has measured electrical properties of flexible PET/ITO substrates up to 11,000 bending times by using FCIS based on the OFRSMC. Measurement results lead to the exponential relation between the width of the line pattern and the change-difference or the change-rate of electrical resistance in tensile or compressive bending. The relationship will be an important reference for flexible electronics research in the future. Accordingly, FCIS is a good tool for inspections of flexible displays under bending. In addition to the electrical property, the present system can also be utilized to measure other properties in bending, e.g., mechanical and optical characteristics, depicted on flexible electronics.

References

Abdallah, C. T., Soualian, V. S., & Schamiloglu, E. (1998). Toward "smart tubes" using iterative learning control. *IEEE Transactions on Plasma Science, 26*(3), 905–911.

Ackermann, J. (1972). Der entwurf linearer regulungs systeme im zustandsraum. *Regelungstechnik und Prozessdatenverarbeitung, 7,* 297–300.

Ahn, H. S., Chen, Y. Q., & Moore, K. L. (2007). Iterative learning control: Brief survey and categorization. *IEEE Transactions on Systems Man and Cybernetics—Part C: Applications and Reviews, 37*(6), 1099–1121.

Alfaro-Cid, E., McGookin, E. W., Murray-Smith, D. J., & Fossen, T. I. (2005). Genetic algorithms optimisation of decoupled sliding mode controllers: Simulated and real results. *Control Engineering Practice, 13*(6), 739–748.

Andrilli, S., & Hecker, D. (2009). *Elementary linear algebra* (4th ed.). Academic Press.

Chang, J. L. (1999). Sliding-mode control design based on conventional pole-assignment method. Ph.D. Dissertation. National Chiao Tung University.

Chen, Y. Q., & Moore, K. L. (2002). A practical iterative learning pathfollowing control of an omni-directional vehicle. *Asian Journal of Control, 4*(1), 90–98.

Chen, Y. Q., Moore, K. L., & Bahl, V. (2004). Learning feedforward control using a dilated b-spline network: Frequency domain analysis and design. *IEEE Transactions on Neural Networks, 15*(2), 355–366.

Cheng, C. C., & Li, T. H. S. (1998). Parallel fuzzy sliding-mode control of a spring-linked cart-pole system. In Proceedings of IEEE IECON'98. Aachen.

Chien, C. J. (2000). A sampled-data iterative learning control using fuzzy network design. *International Journal of Control, 73*(10), 902–913.

Chung, Y. C., Wen, B. J., & Lin, Y. C. (2007). Optimal fuzzy sliding-mode control for bio-microfluidic manipulation. *Control Engineering Practice, 15,* 1093–1105.

Dou, H., Tan, K. K., Lee, T. H., & Zhou, Z. (1999). Iterative learning feedback control of human limbs via functional electrical stimulation. *Control Engineering Practice, 7*(3), 315–325.

Edwards, C., & Tan, C. P. (2006). Sensor fault tolerant control using sliding mode observers. *Control Engineering Practice, 14,* 897–908.

Franklin, G. F., Powell, J. D., & Workman, M. L. (1998). *Digital control of dynamic systems* (3rd ed.). Addison Wesley Longman, Inc.

Gao, W. B., & Hung, J. C. (1993). Variable structure control of nonlinear system: A new approach. *IEEE Transactions on Industrial Electronics, 40*(1), 45–56.

Gao, W. B., Wang, Y., & Homaifa, A. (1995). Discrete-time variable structure control systems. *IEEE Transactions on Industrial Electronics, 42,* 2.

Gonzalez, R. C., & Woods, R. E. (2008). *Digital image processing* (3rd ed.). Prentice-Hall, Inc..

Grego, S., Lewis, J., Vick, E., & Temple, D. (2005). Development and evaluation of bend-testing techniques for flexible-display applications. *Journal of the Society for Information Display, 13*(7), 575–581.

Hung, J. Y., Gao, W. B., & Hung, J. C. (1993). Variable structure control: A survey. *IEEE Transactions on Industrial Electronics, 40*(1), 2–22.

Jiang, P., & Unbehauen, R. (2002). Iterative learning neural network control for nonlinear system trajectory tracking. *Neurocomputing, 48,* 141–153.

Li, T. H. S., & Shieh, M. Y. (2000). Switching-type fuzzy sliding mode control of a cart–pole system. *Mechatronics, 10,* 91–109.

Lin, C. T., & Lee, C. S. (1999). *Neural fuzzy systems.* Prentice-Hall, Inc..

Meier, A. A., & Levinzon, D. I. (1965). Application of the four-probe method for measuring the resistivity of nonuniform semiconductor materials. *Measurement Techniques, 8*(5), 427–429.

Messner, W., Horowitz, R., Kao, W., & Boals, M. (1991). A new adaptive learning rule. *IEEE Transactions on Automatic Control, 36*(2), 188–197.

Ogata, K. (1994). *Discrete-time control systems* (2nd ed.). Prentice-Hall, Inc..

Peng, H., Ozaki, T., Toyoda, Y., & Oda, K. (2001). Exponential ARX model based long-range predictive control strategy for power plants. *Control Engineering Practice, 9,* 1353–1360.

Perl, W. (1960). A method for curve-fitting by exponential functions. *The International Journal of Applied Radiation and Isotopes, 8*(4), 211–222.

Phillips, C. L., & Nagle, H. T. (1995). *Digital control systems analysis and design* (3rd ed.). Prentice-Hall, Inc..

Sinswat, V., & Fallside, F. (1977). Eigenvalue/eigenvector assignment by state feedback. *International Journal of Control, 23,* 183–196.

Slotine, J. J. E., & Li, W. (1991). *Applied nonlinear control.* Prentice-Hall, Inc..

Verhaegen, M., & Verdult, V. (2007). *Filtering and system identification: A least squares approach.* Cambridge University Press.

Wen, B. J., Liu, T. S., Chen, C. H., Ko, H. Y., & Chung, Z. Y. (2008). Measurement method for optical characteristics of flexible vehicle display. In Technical digest of 2008 vehicles and photons symposium, pp. 19–23.

Wu, W. C., & Liu, T. S. (2004). Sliding mode based learning control for track-following in hard disk drives. *Mechatronics, 14,* 861–876.

Xu, J. X., Panda, S. K., & Lee, T. H. (2009). *Real-time iterative learning control: Design and applications* (2nd ed.). Springer-Verlag London Limited.